Journal of Nuclear Materials 390–391 (2009) 818–821

Contents lists available at ScienceDirect

Journal of Nuclear Materials

journal homepage: www.elsevier.com/locate/jnucmat

Power flux in the ITER divertor tile gaps during ELMs

R. Dejarnac [a,*], M. Komm [a], J.P. Gunn [b], R. Panek [a]

[a] Association EURATOM-IPP.CR, Za Slovankou 3, 182 00 Prague 8, Czech Republic
[b] Association EURATOM-CEA Cadarache, 13108 Saint Paul Lez Durance, France

ARTICLE INFO

PACS:
52.40.Hf
52.55.Fa
52.55.Rk
52.65.Rr

ABSTRACT

In order to withstand strong thermo-mechanical stress in the ITER's divertor, its plasma facing components will be castellated. Consequently, a larger area with complex geometry will be exposed to high fluxes coming from the plasma. In order to evaluate the possible damage caused by transient events, we present here calculations of the expected power loads in the ITER divertor tile gaps during ELMs. We use a self-consistent, two-dimensional particle-in-cell technique to model plasma deposition with realistic boundary conditions. The power loads on the tile surface and inside the gaps are investigated for various magnetic configurations of the strike point and strong plasma parameters.

1. Introduction

The objective of this paper is to study the power loads in ITER castellated PFCs by means of kinetic calculations during powerful transient events. We used a three velocity–two-dimensional kinetic code based on particle-in-cell technique [1], which is adapted to such tile gap geometry. The code is based on the resolution of the equations of motion and the integration of Poisson's equation to obtain the self-consistent electric field that accelerates the particles. The novelty of the code is its ability to inject arbitrary velocity distribution functions. For the ions (D^+), we use a non-Maxwellian distribution given by a one-dimensional quasineutral kinetic calculation of the scrape-off layer [2,3] that satisfies the kinetic Bohm criterion at the sheath entrance. However, it has to be noted that this distribution results of a self-consistent calculation with stationary conditions and does not take into account the dynamism of the ELM like with a full PIC model. The velocity is assumed to be constant which is not the case in reality. Nevertheless, we are able to study the plasma power loads to ITER tile gaps taking into account the specific geometry of the components, the inclination of the magnetic field lines and the gyration of the incoming particles. Investigated cases for ELMy H-mode discharges are listed in Table 1.

We simulate two types of gaps according to their orientations with respect to the magnetic field lines. Poloidal Gap (PG) refers to a gap perpendicular to the magnetic field lines and Toroidal Gap (TG) refers to a gap parallel to the magnetic field lines. Both orientations and the incident angle α of the field lines with the surface are shown in Fig. 1. The simulation box includes around 250×100 cells in the maximum case with in average 50 particles per cell ($\approx 4.5 \times 10^6$ particles in the simulation box). The average simulation time was 14.6 days on a 6-processor computer.

2. Power deposition in the gaps

We present here the power profiles in the 0.5 mm ITER divertor gaps for ultimate plasma conditions during ELMs or disruptions described in Table 1. The strike points are defined in the (R,Z) coordinates.

2.1. Effect of the geometrical orientation of the gaps

The power deposition in narrow gaps during ELMs is totally asymmetric in both PG and TG orientations; only one side is wetted by the plasma. In PGs, the wetted side is the plasma facing side, corresponding to the 'lower side' of Fig. 1 and in TGs, the wetted side is the one favored by the $E \times B$ drift. This feature is due to strong gradients of the electric field in the gap as explained in [1]. Moreover, a positive 'bump' on the negative potential forms between the tiles and acts like a regulator for the incoming ion flux according to its size. More or less plasma can enter the gap and might have consequences on the power deposition (see Section 2.2).

Fig. 2 shows typical profiles of the deposited power (P_{gap}) in 0.5 mm gaps for both orientations. The non-perturbed, perpendicular flux falling to the tile surface far from the gap (P_{tile}) is also indicated for reference. At identical plasma conditions ($ne = 10^{20}$ m^{-3}, $Ti = Te = 5$ keV, $Bt = 5.9$ T), we observe that the power load at the entrance (P_{peak}) is higher in PGs (+27%) than in TGs but then decays faster. Moreover, the integrated power along the gap is comparable (within 5%). It means that the same amount

* Corresponding author.
E-mail address: dejarnac@ipp.cas.cz (R. Dejarnac).

0022-3115/$ - see front matter © 2009 Elsevier B.V. All rights reserved.
doi:10.1016/j.jnucmat.2009.01.216

Table 1
Magnetic fields and impact angles of the field lines on the PFCs (ITER design review) for the different geometrical configurations.

	R (m)	***Z*** (m)	B_phi (T)	alpha (°)	ne (m^{-3})	Ti (keV)
1.a. Outer divertor (CFC)	5.5624	−4.4081	5.9094	2.1	5E19 ÷ 1E20	2.5 ÷ 5
1.b. Inner divertor (CFC)	4.0795	−3.7509	8.0502	2.5		
2.a. Outer divertor (CFC)	5.5633	−4.1346	5.9077	1.2	2.5E19 ÷ 5E19	1.2 ÷ 2.5
2.b. Inner divertor (CFC)	4.2932	−3.4993	7.6508	1.5		
3.a. Outer divertor (W)	5.7365	−3.4274	5.7268	1	1E19 ÷ 5E19	0.25 ÷ 1.2

of plasma enters the gap for both orientations but is deposited differently. Here, the total integrated particle flux inside the gap represents 85% of the influx in TGs and 80% in PGs. This result is not geometrically related but is explained by a difference on the size of the potential 'bumps'. Therefore, 15% and 20% of the incoming particles, respectively, do not enter the gap and are deflected to the next tile according to the stream flow.

We also observe that the decay is not exponential. In order to quantify the power deposition inside the gap, we define a deposition length, L_{dep}, as the distance from the gap entrance where the power is 1/1000 P_{peak}. Fig. 2 corresponds to two times a large uncontrolled ELM ($E_{tile} = 4.7$ MJ/m^2 with $\Delta t = 375$ μs) which is a maximum limit, still acceptable for the thermo-mechanical properties of the PFCs. In this case, the power is deposited over $L_{dep} = 0.6$ mm in TGs and $L_{dep} = 0.45$ mm (−22%) in PGs and can be considered as a maximum limit. In the latter case, the penetration is deeper than the geometric projection ($L_{geo} = 0.018$ mm for $\alpha = 2.1°$) and is explained by the gyration of the ions [1]. Profiles for different plasma conditions in TGs are presented in Fig. 3,

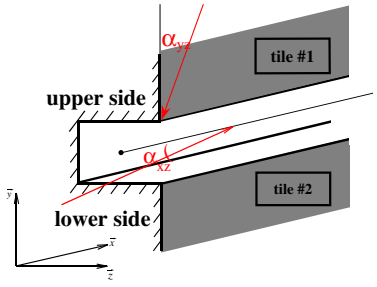

Fig. 1. Scheme of the simulation domain in Cartesian coordinates.

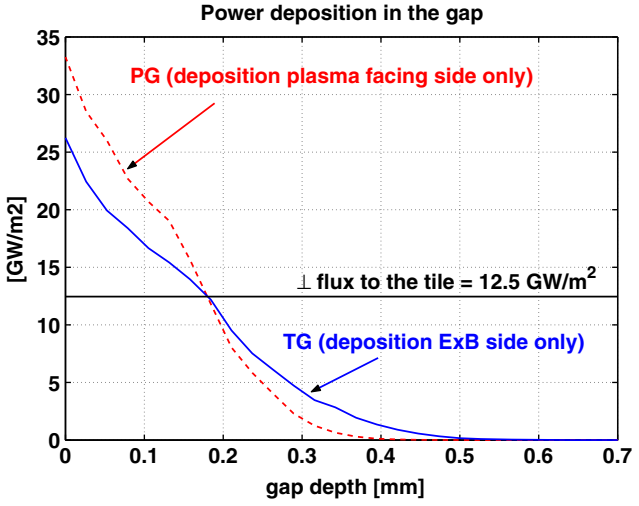

Fig. 2. Power deposition in a 0.5 mm gap when parallel (TG) and perpendicular (PG) to the B-field for 2.1° inclination and ne = 10^{20} m^{-3}, Ti = Te = 5 keV.

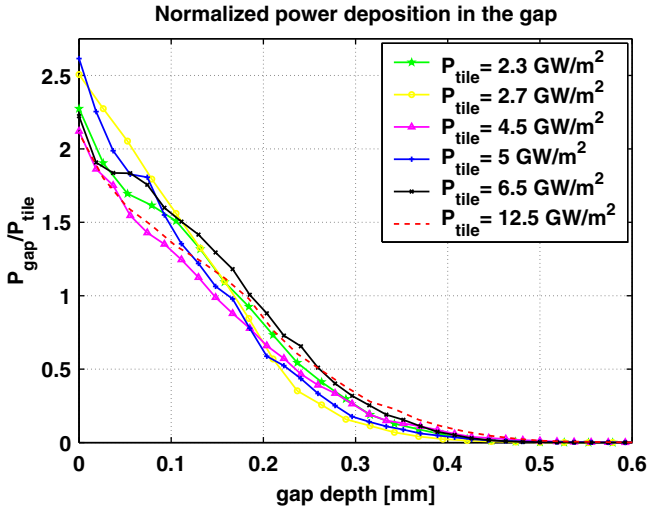

Fig. 3. Normalized power deposition in the TGs of the ITER outer divertor (case 1.a) during ELMs.

corresponding to a power ranging from 2.3 GW/m^2 (∼small uncontrolled ELM) to 12.5 GW/m^2 (∼2x large uncontrolled ELM). The profiles for PGs, with smaller L_{dep}, can be deduced using the trend described previously in Fig. 2. The deposition in the gap varies between $L_{dep} = 0.5$ mm and $L_{dep} = 0.6$ mm, mainly due to the increase of the density. We observe that the peak value varies roughly between 2 and 2.5× P_{tile} for all the cases. The Larmor radii (r_L) are between 3 and 5x bigger than the gap width and almost all the plasma (85% of incoming flux) enters the gap. Concerning PGs, we observe an increase of the peak value by 24% and a decrease of the wetted area by 21% in average. We estimate at 80% the fraction of the plasma that enters the gap for all the similar cases simulated, however, increasing the gap width, at fixed r_L, increases the size of the bump and a bigger fraction of the incoming plasma is deflected to the next tile.

2.2. Effect of the plasma temperature and density

Changing the plasma conditions implies different incoming power fluxes. In order to compare the different effects of the different parameters on the power deposition inside the gaps, we normalize P_{gap} with the non-perturbed perpendicular flux P_{tile}.

Fig. 4(a) shows the normalized power profiles in TGs for two Te in the magnetic configuration of case 1.a. The two profiles are different, with surprisingly a higher P_{peak} for the lower Te, however the deposition lengths are similar. We observe that the power is deposited in the gap over 0.48 mm for Te = 2.5 keV and 0.50 mm for Te = 5 keV. Fig. 4(b) shows similar profiles but for two Ti. We observe that increasing Ti by a factor of 2 changes the profile as in Fig. 4(a) but this time by increasing the peak value. The deposition lengths are similar, $L_{dep} = 0.5$ mm for Ti = 2.5 keV and $L_{dep} = 0.48$ mm for Ti = 5 keV. It has to be noted that the fraction of plasma entering the gap (f_{gap_in}) does not vary extensively with

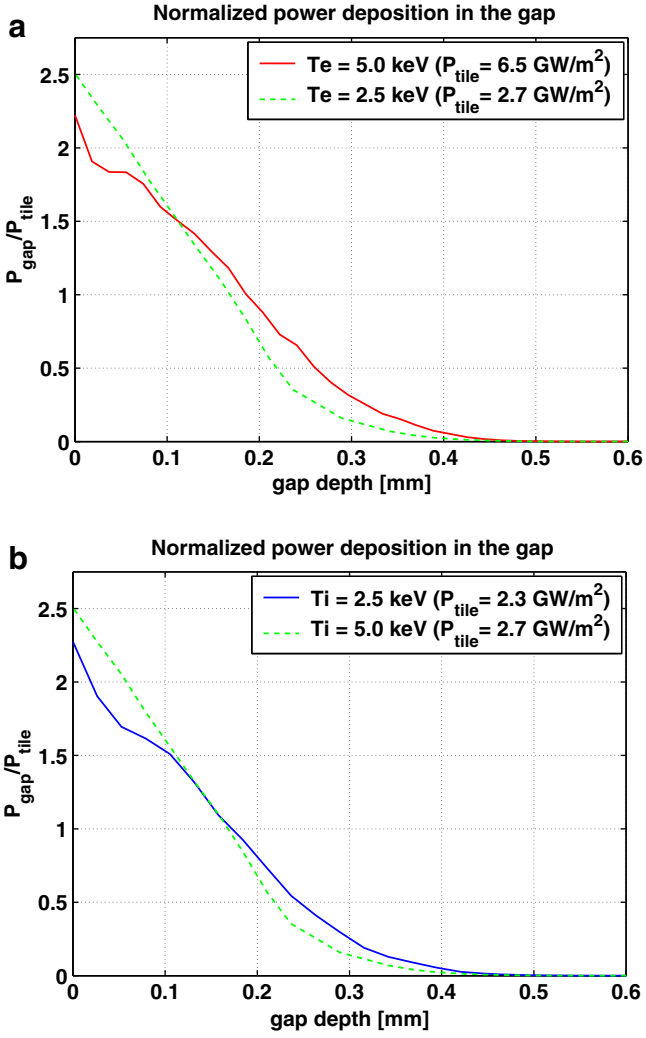

Fig. 4. Effect of Te (a) and Ti (b) on the normalized power deposition in a TG with constant ne = 5×10^{19} m^{-3} and $\alpha = 2.1°$.

Te and Ti in TGs and remains above 75–80%. In PGs, this fraction can vary drastically with the temperature as we can see in Table 2. We notice that L_{dep} increases with f_{gap_in}. By changing the temperature, we modify the Larmor radii and for r_L in the range of the gap width, or smaller, less plasma paradoxically enter the gap. In this case, a charge separation can form inside the gap and a bigger 'bump' on the potential appears than in the case of larger r_L (i.e., bigger than the gap width) where this separation is more difficult to achieve. The bigger the 'bump', the more ions are repelled and do not contribute to the power deposition in the gaps.

The density affects the power deposition profiles in TGs slightly more that the temperature but it remains marginal as we can see in Fig. 5. The power is deposited over L_{dep} = 0.50 mm for ne = 5×10^{19} m^{-3} and by increasing the density by a factor of 2,

Table 2
Power deposition and fraction of the plasma that enters 0.5 mm PGs according to different temperatures (Larmor radii).

Ti = Te (eV)	ne (m^{-3})	P_{tile} (MW/m^2)	r_L (mm)	f_{gap_in}	L_{dep} (mm)
250	10^{19}	16	0.54	55%	0.27
500	10^{19}	45	0.77	65%	0.30
1000	10^{19}	125	1.09	80%	0.32
2000	10^{19}	355	1.55	80%	0.33

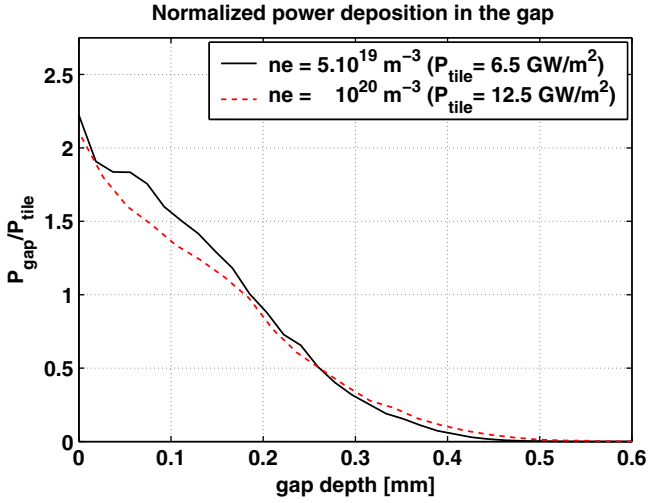

Fig. 5. Effect of ne on the normalized power deposition in a 0.5 mm TG with constant Ti = Te = 5 keV and $\alpha = 2.1°$.

we decrease the deposition length by 16% to reach L_{dep} = 0.58 mm. In PGs, the same trend is observed. At equal power, the deposition will be deeper inside the gap in the case of the higher density.

2.3. Effect of the inclination angle

Fig. 6 shows the normalized power profiles in TGs for two angles, $\alpha = 2.1°$ (dashed line) & $\alpha = 1.2°$ (full line), and for similar plasma conditions (ne = 5×10^{19} m^{-3}, Ti = Te = 2.5 keV, Bt = 5.9 T). The fluxes falling to the tile surface are in a ratio of a factor of 2 due to the different angles. However, the decrease of the wetted area inside the gap is only by 30%. We have L_{dep} = 0.50 mm for $\alpha = 2.1°$ whereas the deposition is L_{dep} = 0.35 mm for $\alpha = 1.2°$. Concerning the local value at the entrance, P_{peak} increases, relatively to the P_{tile}, with smaller angle but remains nevertheless lower in absolute value. We can note that the integrals of the curves shown in Fig. 6 are identical due to those two features. This means that the total power inside the gaps is only dependant on the incoming power to the tiles. The same conclusions concerning the effect of the incident angle apply to the PGs. The curves are similar and the only

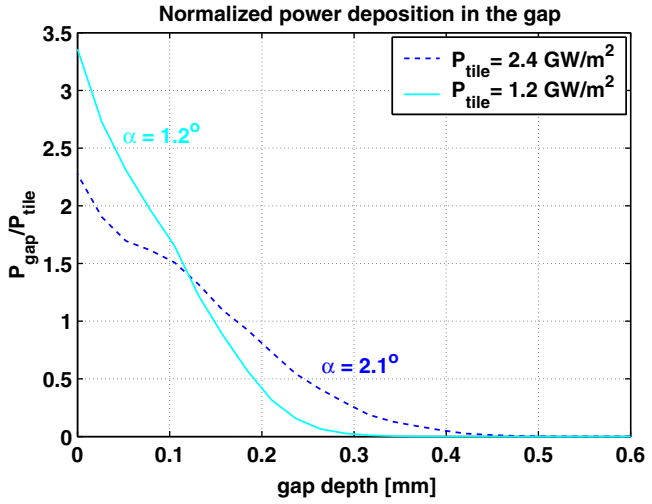

Fig. 6. Normalized power deposition in a 0.5 mm TG for an inclination angle of 2.1° (dashed line) and 1.2° (full line) at identical plasma conditions.

difference comes from the geometric effect described in Section 2.1 according to Fig. 2 trend.

3. Conclusion

The plasma deposition in gaps between tiles of ITER PFCs during ELMs is strongly asymmetric. In PGs, the wetted area is the plasma facing side and in TGs, the plasma deposition is made on the side favored by the E × B drift. We observe that the local power load at the entrance of the gap is higher in PGs than in TGs but is globally deposited on a shorter distance. Moreover, a positive 'bump' on the negative potential can form under certain circumstances (weak plasma conditions, large gaps compared to r_L, wide incident angles). This potential 'bump' acts like a regulator and can let more or less plasma in the gap according to its size. It amplifies the process that consists of diminishing L_{dep} and increasing P_{peak}, initiated by the different orientations, especially in the case of PGs. The second drawback is that the fraction of ions that does not enter the gap is deposited on the following tile according to the plasma flow. This has to be taken into account for thermo-mechanical purposes. The power can be raised on the next tile by 20% minimum compared to the unperturbed perpendicular flux. The inclination angle of the magnetic field lines with respect to the tile surface plays an important role in the power deposition inside gaps. Decreasing the angle reduces strongly the deposition inside the gaps for both orientations. The main drawback is a strong increase of the peak value at the entrance of the gap. Finally, the intuitive idea that smaller gaps collect less plasma than larger gaps is confirmed.

The temperature does not affect strongly L_{dep} in TGs, whereas increasing the density implies a slightly deeper deposition inside the gap. At equal power, the deposition will be deeper inside the gap for the higher density. For PGs, the temperature has a strong effect on L_{dep} via the fraction of plasma that enters the gap, which is inverse proportional to the size of the potential 'bump'. The density effect is similar to TGs. Generally, we can say that the deposition in the gaps is generally made on a distance of the same order than the gap width.

Acknowledgments

This work was supported by the Grant Agency of the Academy of Sciences of the Czech Republic No. GA AV B100430602 and is part of the EFDA Technology Workprogramme TW6-TPP-DAMTRAN.

References

[1] R. Dejarnac, J.P. Gunn, J. Nucl. Mater. 363–365 (2007) 560.
[2] V. Fuchs et al., in: Thirty Second EPS Physics Conference, Tarragona, 2005.
[3] J.P. Gunn, V. Fuchs, Phys. Plasmas 14 (2007) 032501.